Single-cell analysis of bovine muscle-derived cell types for cultured meat production

Tobias Messmer[1,2], Richard GJ Dohmen[1,2], Lieke Schaeken[1], Lea Melzener[1,2], Rui Hueber[1], Mary Godec[1], Mark J Post[1,2], Joshua E Flack*[1]

Affiliation: [1]Mosa Meat, [2] Maastricht University

Keywords: single-cell RNA sequencing, cultured meat, cell purification, muscle stem cells, satellite cell heterogeneity

Abstract

'Cultured' meat technologies leverage the proliferation and differentiation of animal-derived stem cells *ex vivo* to produce edible tissues for human consumption in a sustainable fashion. However, skeletal muscle is a dynamic and highly complex tissue, involving the interplay of numerous mono- and multinucleated cells, including muscle fibres, satellite cells (SCs) and fibro-adipogenic progenitors (FAPs), and recreation of the tissue *in vitro* thus requires the characterisation and manipulation of a broad range of cell types. Here, we use a single-cell RNA sequencing approach to characterise cellular heterogeneity within bovine muscle and muscle-derived cell cultures over time. Using this data, we identify numerous distinct cell type, and develop robust protocols for the easy purification and proliferation of several of these populations. We note overgrowth of undesirable cell types within heterogeneous proliferative cultures as a barrier to efficient cultured meat production, and use transcriptomics to identify conditions that favour the growth of SCs in the context of serum-free medium. Combining RNA velocities computed in silico with time-resolved flow cytometric analysis, we characterise dynamic subpopulations and transitions between active, quiescent, and committed states of SCs, and demonstrate methods for modulation of these states during long-term proliferative cultures. This work provides an important reference for advancing our knowledge of bovine skeletal muscle biology, and its application in the development of cultured meat technologies.

Introduction

'Cultured' or 'cultivated' meat is an emergent technology that leverages in vitro proliferation and differentiation of stem cells to produce edible tissues that mimic conventional meat[1,2]. Whilst there are numerous potential advantages to this technology, including reduced greenhouse gas emissions and improved animal welfare[3], many technical challenges remain, such as the removal of animal-derived components, scaling of culture volumes, and cost reduction[4,5]. Moreover, consumer acceptance will be reliant on the taste and texture of cultured meat products closely replicating those of the conventionally-reared equivalent[6,7].

Meat is composed primarily of skeletal muscle, a complex tissue whose function requires the interplay of numerous mono- and multinucleated cell types, including muscle fibres, satellite cells (SCs) and fibro-adipogenic progenitors (FAPs), as well as vascular, nervous and connective tissue[8,9]. Whilst most cultured meat products currently being pursued consist of unstructured muscle fibres, with or without fat tissue, accurate recreation of the entire tissue requires the identification, purification, proliferation and characterisation of a broad range of cell types[10,11]. Descriptions of the composition of human and murine skeletal muscle at the cellular level are now available[12–16], but a similarly detailed understanding of muscle biology in agriculturally relevant species, such as cattle, is currently lacking. Furthermore, the extent to which complex muscle-derived cell behaviours and interactions are recapitulated during in vitro culture is unclear[17,18], limiting the progress of cultured meat development.

Here, we used droplet-based single-cell RNA sequencing (scRNA-seq) to profile bovine skeletal muscle, and muscle-derived cell cultures, in a time-resolved fashion across the process of cultured meat production. We use the resultant dataset to gain insight into transcriptional heterogeneity between and within cell types, and to inform various steps of cultured meat bioprocess design.

53 # Results

54 **scRNA-seq identifies 11 distinct cell types in bovine muscle**

55

56 In order to investigate heterogeneity between and within bovine muscle-derived cell types, we
57 used the 10x Chromium platform for scRNA-seq to study gene expression at five timepoints in a
58 primary adult stem cell-based cultured meat production process (Fig. 1a, Supplementary Table
59 1). A total of 36129 single-cell transcriptomes, with an average expression of 3815 genes and
60 21131 transcripts per cell, were analysed across 10 donor cattle and assembled into a single
61 dataset (Supplementary Fig. 1). Using UMAP dimensionality reduction, based on the first 30
62 principal components (Fig. 1b), cells from Timepoints 1 (muscle tissue) and 2 (passage 0, after
63 72 h in vitro culture) clustered separately from each other, and from Timepoints 3 to 5 (after
64 passages 2, 5 and 8 respectively), indicating significant transcriptomic changes between
65 timepoints and within cell types during the proliferative process.

66

67 Within enzymatically digested bovine muscle tissue (Timepoint 1), we identified 11 defined
68 populations of mononuclear cells with distinct gene expression profiles (Fig. 1c; Supplementary
69 Table 2), which were present in varying proportions in all donor animals (Supplementary Fig. 2a).
70 Based on differential gene expression, these clusters were assigned to cell types previously
71 characterised in other species[12,13,19], namely fibro-adipogenic progenitors (FAPs), satellite cells
72 (SCs), vascular and lymphatic endothelial cells (ECs; vascular, VECs; lymphatic, LECs,
73 Supplementary Fig. 2b), smooth muscle and mesenchymal cells (SMMCs),
74 monocytes/macrophages (MΦ), neutrophils, lymphocytes (B/T/NK cells), glial cells, tenocytes and
75 myocytes (Fig. 1d, Supplemental Fig. 2d). The expression of canonical genes in each of these
76 populations in analogous studies indicated their conservation between mouse and cattle (Fig. 1e,
77 Supplemental Fig. 2e)[14].

Cell types can be identified in vitro by unique surface marker expression

In order to identify proliferative muscle tissue-derived cell types that might be used for cultured meat production, we analysed the adherent cell fraction after 72 h (Timepoint 2) culture in serum-free growth medium (SFGM, Supplementary Table 3). We discerned 7 populations present in these cultures, which were separated from the same populations in Timepoint 1 by UMAP, indicating stark transcriptional changes during the transition to in vitro culture (Fig. 2a). GO terms corresponding to differentially expressed genes (independent of cell type) between Timepoints 1 and 2 (Fig. 2b) suggest that these transcriptional switches relate to decreased interaction with the extracellular matrix (ECM) and increased protein production, concomitant with increased cellular proliferation in the in vitro environment.

Comparison of Timepoints 1 and 2 enabled the assigning of cell identities to individual clusters (Fig. 2c), indicating that of the 11 populations identified in Timepoint 1, only myocytes, tenocytes, neutrophils and lymphocytes did not persist in short-term serum-free culture. Conversely, FAPs, SCs, SMMCs, ECs, glial cells and monocytes/macrophages remained present in cultures from all genotypes (donor animals) sequenced (Supplementary Figs. 3a, b). These same cell types were identified when culturing cells in growth medium (GM) containing 20% foetal bovine serum (FBS; Supplementary Fig. 3c, Supplementary Table 3), indicating that our SFGM formulation was able to support culture of muscle-derived cells as robustly as traditional serum-containing media.

Analysis of differentially expressed genes yielded highly and exclusively expressed markers for each population (Fig. 2d)[10,20] that have previously been described in mouse and human[12–14,21]. Filtering these lists for genes encoding plasma membrane-localised proteins facilitated the identification of candidate cell surface markers for separation of populations by flow cytometry (Fig. 2e). Staining of muscle tissue-derived cells 72 h post-isolation for JAM-1 (*F11R*), CD45 (*PTPRC*), ITGA7 and ITGA5 confirmed the suitability of this quartet of markers as a FACS panel (Fig. 2f, Supplementary Fig. 3d).

106 **Four principal muscle-derived cell types can be proliferated in vitro**

107

108 In order to characterise their in vitro phenotypes in more detail, we sorted muscle-derived cells
109 into FAPs, SCs, ECs and SMMCs using the FACS panel previously described (Fig. 2). The
110 purified populations exhibited markedly different morphologies; whilst FAPs had a spindle-like
111 morphology and SCs were more spherical, ECs and SMMCs appeared flatter and larger (Fig. 3a).
112 Flow cytometric analysis post-FACS using the same antibody panel confirmed high sorting
113 purities for all populations (Fig. 3b). In addition, immunofluorescent staining for canonical markers
114 PDGFRα, Pax7, TEK (also known as Tie2), and Calponin-1 (CNN1) further verified the identity of
115 FAPs, SCs, ECs, and SMMCs respectively (Fig. 3c).

116

117 Long-term proliferation of each of these populations was supported in SFGM (FAPs, SCs) or
118 BioAMF-3 medium (ECs, SMMCs), with each culture undergoing at least 15 population doublings
119 (PDs) over a period of at least 6 passages (Fig. 3d). Proliferation rates varied between cell types
120 (for example, from 0.46 (ECs) to 1.0 PDs/day (SMMCs) at early passage), and tended to decrease
121 over time (Fig. 3e).

122 **Optimised culture conditions prevent SC overgrowth by FAPs**

123

124 We next aimed to understand heterogeneity within FACS-purified SC cultures during long-term
125 proliferation. Surprisingly, we found that cells in these cultures clustered into two distinct
126 populations, marked by differential expression of *ITGA7* (Fig. 4a). *ITGA7*- cells expressed FAP
127 marker genes such as *ITGA5* (Supplemental Fig. 4a, Fig. 2), suggesting that these cells were
128 FAPs that were inaccurately sorted into, and remained prevalent within, SC cultures.
129 Quantification of these cell types showed that the proportion of FAPs increased over time,
130 indicating that our standard culture conditions favoured long-term proliferation of FAPs over SCs
131 (Fig. 4b, Supplemental Fig. 4b). The percentage of contaminating FAPs correlated negatively with
132 myogenic differentiation, as determined by fusion index (Figs. 4c, d), emphasising the importance
133 of eliminating overgrowth by non-SCs for cultured muscle production.

134

135 We therefore sought to adapt the long-term culture conditions, with the aim of preventing FAPs
136 from overgrowing SCs. To inform our approach, we filtered the scRNA-seq data for differentially
137 expressed genes between SCs and FAPs encoding receptors that interact with proteins
138 commonly used as surface coatings or growth factors, revealing a number of interesting
139 candidates (Fig. 4e, f). Sorting SCs using an ITGA7+/ITGA5- strategy significantly decreased FAP
140 contamination as compared to a CD29+/NCAM1+ sorting strategy (used in previous studies[22]),
141 reducing FAP overgrowth after multiple passages (Figs. 4g, h). Culturing SCs contaminated with
142 FAPs on different coatings, we observed that within 3 passages, SC purity was reduced on
143 collagen I and fibronectin (FN; interacting with ITGA5) but remained high on laminin-521 (LN-521;
144 interacting with ITGA7; Fig. 4i). We further adapted SFGM by adding triiodothyronine (T3, 30 nM,
145 ligand for THRA), increasing the concentration of HGF (ligand for c-Met) and removing PDGF-BB
146 (ligand for PDGFRα; Fig. 4j). Each individual adaptation reduced FAP overgrowth over 3
147 passages, whilst the combination of all three showed no significant reduction in SC proportion
148 over the course of the experiment, and was thus labelled 'improved SFGM' (i-SFGM).

149 **SCs transition between three dynamic states**

150

151 To further investigate SC heterogeneity in vitro, we filtered out FAPs and reanalysed the
152 remaining single-cell transcriptomes at passage 2 (Timepoint 3). Reclustering identified three
153 subpopulations within SCs, with distinct gene expression profiles suggestive of quiescent,
154 activated, and committed states (similar to those previously observed in murine SCs[14]; Figs. 5a,
155 b). Genes encoding proteins related to focal adhesion and ECM organisation were upregulated
156 in the quiescent state, cell cycle and replication in the activated state, and myogenic differentiation
157 the committed state (Fig. 5c, Supplementary Fig. 5a). These cell states were also observed at
158 passages 5 and 8, but in different ratios (Supplementary Figs. 5b, c), suggesting the possibility of
159 transitioning between states.

160

161 We next established protocols to measure these states in vitro, through analysis of CD151
162 (upregulated in quiescent SCs[14]) and desmin (upregulated in committed SCs) via flow cytometry
163 (Fig. 5d, Supplementary Fig. 5d). Combining this panel with EdU-staining, we confirmed
164 increased cell cycle activity in activated as compared to quiescent SCs (Fig. 5e; Supplementary
165 Fig. 5e). Investigating the dynamics of these subpopulations during a single passage, we found
166 dynamic conversion between quiescent (CD151+) and activated (CD151-) states, with an initial
167 increase in quiescent SCs followed by a rapid decline and a renewed increase as cells approach
168 confluence (Fig. 5f). The proportion of cells in the committed state remained stable throughout
169 the first 72 h, increasing after 96 h. Investigating over multiple passages revealed that this
170 interchangeability decreased over time (Supplementary Fig. 5f). We observed that i-SFGM
171 increased the proportion of activated SCs compared to SFGM, both within a single passage (Fig.
172 5f) and over the course of multiple passages (Supplementary Fig. 5f). In addition to transitions
173 between cell states changing over the course of cell aging, transcriptional changes related to
174 increased ECM remodelling and decreased translation were also observed *within* states over time
175 (Supplementary Fig. 6).

176

177 Finally, we performed RNA velocity analysis of SCs at passage 2, in order to investigate these
178 cell state transitions in silico. RNA velocity averaged across all genes indicated transitions from
179 the activated to the quiescent state or committed states (Fig. 5g), whilst an increase in expression
180 of cell cycle genes within a subset of quiescent cells suggested they are able to return to the
181 activated state (Fig. 5h). Taken together with in vitro data, this suggests a dynamic, reversible

182 transition between activated and quiescent states, whilst activated cells can also differentiate
183 towards committed myocytes as SCs become confluent (Fig. 5i).

184 # Discussion

185 The complexity of muscle tissue arises from the interplay of multiple cell types[8,9]. Here, we have
186 presented an annotated scRNA-seq dataset comprising over 36,000 muscle cellular
187 transcriptomes, from 10 donor cattle, across five timepoints during a cultured beef production
188 process. This dataset gives significant insight into the cellular heterogeneity present in bovine
189 skeletal muscle for the first time, including comprehensive analysis of 11 defined cell types (Fig.
190 1). Our analysis showed notable similarity between bovine muscle and analogous approaches
191 employed for more well-studied species, with expression of canonical genes for distinct cell types
192 largely conserved between cattle, human and mouse. Comparison of bovine muscle with the
193 corresponding cell cultures shed light on transcriptional changes that occur during the transition
194 to in vitro culture. Notably, genes related to protein synthesis were strongly upregulated
195 (suggesting cell activation), whilst those relating to ECM were downregulated, highlighting the
196 pivotal role of cell-matrix interactions in the muscle niche. However, despite the absence of
197 signalling from the microenvironment, the expression of most canonical marker genes was
198 conserved in vitro (Fig. 2), suggesting that muscle-derived cell cultures are able to recapitulate in
199 vivo behaviour to a large extent.
200
201 Differential expression analysis allowed us to identify surface marker panels for physical
202 separation of multiple cell types, including SCs, FAPs, ECs and SMMCs (together representing
203 over 80% of mononucleated cells). Notably, inclusion of ITGA5 in the panel offered significant
204 purity improvements over previous protocols, as this integrin serves as a negative selection
205 marker for SCs, whilst ITGB1/CD29 (previously used as a SC marker[22,23]) is highly expressed by
206 both SCs and FAPs. Whilst we were able to proliferate each of these cell types for multiple
207 passages (Fig. 3), further work is needed to assess the potential of ECs and SMMCs, with respect
208 to their long-term proliferation in the absence of FBS and their capacity to promote myogenesis
209 or adipogenesis, for example in co-culture systems[12,24]. Other low-abundance cell types, such as
210 macrophages, could also offer benefits in terms of tissue remodelling and angiogenesis for
211 structured cultured meat products[25,26].
212
213 Cultured meat production requires an extensive proliferation phase, with many PDs, to achieve
214 required cell yields[5]. This prompts several issues, including reduced growth rates, loss of
215 differentiation capacity, and the possibility of overgrowth of undesired cell types. Transcriptomic
216 analysis indeed revealed that sorted SCs were rapidly overgrown by a small proportion of

217 contaminating FAPs, indicating variable growth dynamics in our initial culture conditions that
218 favour FAP proliferation (Fig. 4). Whilst high levels of animal-derived sera have traditionally been
219 used to control fibroblastic overgrowth in SC cultures[27], this phenomenon is poorly understood,
220 and in any case is unsuited for cultured meat applications. We used differential expression
221 analysis to inform several improvements to the SC culture conditions, including the switch to an
222 ECM mimic that corresponds to the integrin expression profile of SCs (laminin is known to interact
223 with ITGA7/ITGB1 dimers[28]), and the addition of growth factors, such as HGF, whose receptor
224 expression is specific to SCs[29,30]. Our dataset will also provide insights into design of selective
225 media for other cell types, such as ECs, which is likely complicated by their slow proliferation.
226 Detailed metabolic profiling, which was beyond the scope of this study, could help to further inform
227 the design of feeding strategies that afford efficient and selective growth of desired cell types[31]. It
228 should be noted that our experiments are conducted at lab scale, and that proliferation in
229 bioreactor systems used for upscaled cultured meat production will introduce additional stresses,
230 that could act differentially across cell types[32]. Further cost reduction will also be required, and
231 our dataset can assist in the replacement of growth and attachment factors with peptide
232 alternatives with retained (or superior) cell type selectivities.
233
234 Our transcriptomic analysis also revealed remarkable heterogeneity *within* cell types, notably
235 between distinct subpopulations of SCs, that points towards a dynamic equilibrium of quiescent,
236 active and committed states (Fig. 5). Different SC states have previously been proposed, both
237 from dissociated muscle samples[15,33–35] and in vitro cultures[16,36,37], although without clear
238 consensus. We identified CD151 (previously observed in human skeletal muscle[13]) as a cell-
239 surface marker for the 'quiescent' cluster, although the extent to which the quiescent phenotype
240 we observed in vitro reflects physiological SC behaviour during embryonic development or wound
241 healing remains unclear. We did not distinguish such states in our bovine muscle samples,
242 perhaps because the majority of cells are activated during tissue dissociation[33]. RNA velocity
243 analysis suggests a model in which only activated SCs are able to differentiate, which is congruent
244 with a physiological model of wound healing in which activated SCs either differentiate to form
245 muscle fibres, or return to a quiescent state in order to preserve the ability of the tissue to respond
246 to future regenerative stimuli. However, higher resolution velocity analysis of SCs would be
247 informative, given that we only sampled a snapshot within each passage (when cells were
248 approaching confluency). Indeed, the role that confluency plays in the promotion of differentiation,
249 and the extent to which premature differentiation might negatively affect a proliferative culture,
250 requires further study in the context of a cultured meat bioprocess design. Similarly, whilst

251 increased culture length clearly affects the transitions of SCs between states, it is important to
252 note that we also observed substantial transcriptomic differences between equivalent states at
253 different timepoints (Supplementary Fig. 6), indicating that cellular aging cannot be understood
254 solely in terms of subpopulation ratio changes. Indeed, our data supports the hypothesis that a
255 reduced rate of switching between states could be a characteristic of SC aging or senescence[38,39].
256 Future transcriptomic experiments, including single-nuclei approaches, could illuminate the
257 formation of cultured muscle tissues during the differentiation of SCs. Furthermore, although not
258 specified in this study, it is likely that similar cellular heterogeneity is present in other cell types,
259 including FAPs, where adipogenic and fibroblastic fate decisions could be critical for cultured fat
260 production[40,41].
261
262 In conclusion, scRNA-seq is a powerful approach to study cell heterogeneity in the context of
263 cultured meat production. Our dataset offers a number of important insights for cell purification
264 and proliferation steps, has led to the development of refined medium conditions, and represents
265 a useful resource for further analysis and improvement of cultured meat bioprocesses.

266 # Material & Methods

267

268 **Cell isolation**

269 Cells were isolated from semitendinosus muscles of 10 Belgian Blue cattle (Supplementary Table
270 1) by collagenase digestion (CLSAFA, Worthington; 1 h; 37 °C), filtration with 100 µm cell
271 strainers, red blood lysis using a Ammonium-Chloride-Potassium (ACK) lysis buffer, and final
272 filtration with 40 µm cell strainers. Cells from each donor animal were plated as separate cultures
273 in serum-free growth medium[42] (SFGM, Supplementary Table 3) on fibronectin-coated (4 µg cm^{-}
274 ^{2} bovine fibronectin; F1141, Sigma-Aldrich) tissue culture vessels for 72 h prior to FACS, or (where
275 denoted) in growth medium (GM) containing 20% foetal bovine serum (heat-inactivated FBS;
276 10500-064, Gibco).

277

278 **Cell culture**

279 Tissue culture vessels were coated with fibronectin for unsorted cells, ECs, and SMMCs, laminin-
280 521 (0.5 µg cm^{-2}, LN521-05, Biolamina) for SCs, or collagen I (0.6 µg cm^{-2}, bovine skin collagen;
281 C2124, Sigma-Aldrich) for FAPs for 1 h prior to plating. Unsorted cells, SCs and FAPs were
282 cultured in SFGM (except where otherwise noted), and passaged every 3-4 days upon reaching
283 confluency. ECs and SMMCs were cultured in BioAMF-3 (01-196-1A, Sartorius).

284

285 To assess long-term proliferation, cells were cultured as described above for each cell type. Cells
286 were harvested upon approaching confluence, counted, reseeded at $5x10^{3}$ cm^{-2} and purity
287 assessed at each passage via flow cytometry.

288

289 **Single cell RNA-sequencing**

290 *Cell harvesting*

291 Five timepoints throughout long-term in vitro culture were selected for single-cell RNA sequencing
292 (scRNA-seq), for each of which cells from all genotypes (donor animals) were pooled in equal
293 ratios and washed with 1% BSA in PBS prior to injection. Timepoints 1 to 5 corresponded to
294 unsorted cells directly after isolation ('Muscle') and after 72 h ('passage 0'), and to cultured cells
295 (unsorted cells, SCs and FAPs) at passages 2, 5, and 8 respectively (Fig. 1a, Supplementary
296 Table 1).

297

298 *Library preparation and sequencing*

299 25000 cells were injected for each timepoint into Chromium Single Cell Controller, emulsified with
300 bar-coded gel beads and libraries were constructed following the protocol of the Chromium
301 NextGEM Single Cell 3' Kit V3.1 (10x Genomics). Quality control of the DNA library was performed
302 on Qiaxcel (QIAgen) and quantified by qPCR using the KAPA SYBR Fast qPCR Master Mix
303 (Illumina). Paired- end single cell 3' gene expression libraries were sequenced on a Novaseq
304 6000 System (Illumina) using a NovaSeq S1 flow-cell to a depth of at least 3.5 x 10^8
305 reads/timepoint.
306
307 *Data processing and demultiplexing*
308 Raw base call files were demultiplexed using the cellranger mkfastq function (CellRanger 6.0.1).
309 Reads were aligned to Bos Taurus genome (build ARS-UCD1.2) with Ensembl annotations
310 (release 101), using CellRanger count function. Default filtering parameters of CellRanger were
311 applied to obtain a gene expression matrix. Genotypes were deconvolved and assigned to
312 individual cells using demuxlet[43], based on VCF files previously generated by genotyping of each
313 donor animal with a BovineSNP50 v3 DNA Analysis BeadChip (Illumina).
314
315 *Quality control and normalisation*
316 Across the five timepoints, 36129 cells (90.8%) passed quality control (within 3 median absolute
317 deviations of the median for expressed genes, total counts and percentage mitochondrial genes;
318 Supplementary Fig. 1). Counts for each timepoint were normalised using the sctransform function
319 of Seurat with default parameters[44,45], regressing out percentage of mitochondrial genes, library
320 size, number of genes, and cell cycle effects.
321
322 *Dimensionality reduction and differential gene expression analysis*
323 Cells were clustered using the FindNeighbors() and FindClusters() functions based on the first 50
324 principal components and with a resolution of 0.1 respectively. Dimensionality was reduced by
325 uniform manifold approximation and projection (UMAP)[46] using the first 30 principal components
326 as input, 50 neighbouring points and a minimal distance of 0.1).
327
328 Differentially expressed (DE) genes were computed for clusters identified in each timepoint by
329 using the FindAllMarkers(), or between denoted conditions using FindMarkers(), with a $\log_2$ fold-
330 change (log-FC) threshold of 1, a false discovery rate (FDR) of 0.05, and expressed in at least
331 50% of cells. For Timepoint 1, cell types were assigned to each cluster based on DE genes and
332 on predicted phenotypes from FindTransferAnchors()[47] using analogous murine scRNA-seq data

333 (GSE143437[14]). ECs were further characterised by their expression of signatures derived from
334 the Descartes human genes expression atlas[19] using the AddModuleScore function. For
335 Timepoint 2, surface markers amongst the DE genes were identified by filtering for genes coding
336 for proteins located in the plasma membrane[48]. GO terms for biological processes (2021) were
337 computed using enrichR[49]. For the analysis of SC cultures, Timepoints 3 to 5 were filtered for
338 genotypes 5, 6, and 10 (Fig. 4), whilst for analysis of SC states these were further filtered by
339 removal of *ITGA5*+ FAP clusters (Fig. 5).
340
341 *RNA velocity analysis*
342 RNA velocities were computed for SCs at Timepoint 3 by generating separate count matrices for
343 spliced and unspliced transcripts using velocyto. The resulting loom files were analysed using
344 scVelo in Python 3.9.12. Transcription kinetics for selected genes were computed, as well as RNA
345 velocity vectors (based on the scVelo dynamical model) across all genes[50,51].
346
347 **Flow cytometry**
348 For cell type identification, unsorted cells were stained for ITGA5, ITGA7, JAM-1 and CD45 (Fig.
349 3, Supplementary Table 4) for 15 min prior to analysis on a MACSQuant10 Flow Analyzer (Miltenyi
350 Biotec). To determine proportions of SCs and FAPs (Fig. 4), cells were stained for ITGA7 and
351 ITGA5. For analysis of SC states (Fig. 5), cells were stained for CD151 prior to fixation (PFA),
352 permeabilisation (10% saponin), and staining for desmin. Samples were subsequently washed
353 and stained with α-mouse-PE secondary antibodies prior to analysis.
354
355 **Fluorescent-activated cell sorting (FACS)**
356 Cells were purified by FACS 72 h post-isolation on a MACSQuant Tyto Cell Sorter (Miltenyi
357 Biotec) following antibody staining as described above. SCs, FAPs, SMMCs and ECs were gated
358 as described in Fig. 2. Where noted, cells were gated for NCAM1+/CD29+ (Fig. 4g).
359
360 **Immunofluorescent staining**
361 After formaldehyde fixation, cells were permeabilised (0.5% Triton X-100), blocked (2% bovine
362 serum albumin (BSA)) and stained with PDGFRα, Pax7, TEK, and CNN1 (for phenotype
363 confirmation; Fig. 3c) or desmin (for fusion index; Fig. 4c) primary antibodies (see Supplementary
364 Table 4). After washing, cells were incubated with AF488-conjugated secondary antibodies and
365 Hoechst 33342 (Thermo Fisher) prior to imaging on an ImageXpress Pico Automated Cell
366 Imaging System (Molecular Devices).

367

368 **Myogenic differentiation assay**

369 Mixed cultures containing SCs and FAPs in varying proportions were seeded on 0.5% Matrigel-
370 coated vessels at a density of $5x10^4$ cm^{-2} in SFGM for 24 h, before switching to serum-free
371 differentiation media (SFDM). After 72 h in SFDM, cells were fixed with 4% formaldehyde, stained
372 for desmin and imaged as previously described. To calculate fusion indices, number of nuclei
373 within desmin-stained areas were divided by total nuclei.

374

375 **Cell cycle analysis**

376 For flow cytometric cell cycle analysis, SCs were incubated with EdU for 90 min prior to
377 trypsinisation. Following α-CD151-APC staining, Click-iT reaction was performed using the Click-
378 iT EdU Alexa Fluor 488 Flow Cytometry Assay Kit (C10420, Thermo Fisher) according to the
379 supplier's protocol, followed by α-desmin staining as previously described. Finally, the cells were
380 gated into quiescent ($DES^-/CD151^+$) and activated ($DES^-/CD151^-$) and within these, into EdU^+ (S-
381 Phase), $DAPI^{low}/EdU^-$ (G0/1-Phase) and $DAPI^{high}/EdU^-$ (G2-Phase), as shown in Supplementary
382 Fig. 5d.

383

384 **Statistical analyses**

385 Statistical analyses were performed using Prism 9 (Graphpad). Pearson correlation of fusion
386 indices with percentages of ITGA7+ cells was computed assuming a normal distribution (Fig. 4d).
387 For comparisons of culture conditions (Figs. 4h-j) and the analysis of cell cycle states in SCs (Fig.
388 5e), two-way ANOVAs were performed including post-hoc Tukey's multiple comparison test.
389 Sample replicates consisted of cells from the same donor animal, cultured in separate vessels.

390

391 **Data availability**

392 scRNA-seq data is deposited in the NCBI Gene Expression Omnibus database (accession code
393 GSE211428).

394

395 **Code availability**

396 Code for scRNA-seq analysis (including RNA velocity calculations) are available from the authors
397 on request.

Bibliography

1. Post, M. J. Cultured beef: medical technology to produce food. *J. Sci. Food Agric.* **94**, 1039–1041 (2014).
2. Datar, I. & Betti, M. Possibilities for an in vitro meat production system. *Innov. Food Sci. Emerg. Technol.* **11**, 13–22 (2010).
3. Parodi, A. *et al.* The potential of future foods for sustainable and healthy diets. *Nat. Sustain.* **1**, 782–789 (2018).
4. Post, M. *et al.* Scientific, sustainability and regulatory challenges of cultured meat. *Nat. Food* **1**, 403–415 (2020).
5. Melzener, L., Verzijden, K. E., Buijs, A. J., Post, M. J. & Flack, J. E. Cultured beef: from small biopsy to substantial quantity. *J. Sci. Food Agric.* **101**, 7–14 (2021).
6. Wilks, M., Phillips, C. J. C., Fielding, K. & Hornsey, M. J. Testing potential psychological predictors of attitudes towards cultured meat. *Appetite* **136**, 137–145 (2019).
7. Bryant, C. & Barnett, J. Consumer acceptance of cultured meat: A systematic review. *Meat Sci.* **143**, 8–17 (2018).
8. Mukund, K. & Subramaniam, S. Skeletal muscle: A review of molecular structure and function, in health and disease. *Wiley Interdiscip. Rev. Syst. Biol. Med.* **12**, e1462 (2020).
9. Forcina, L., Miano, C., Pelosi, L. & Musarò, A. An Overview about the Biology of Skeletal Muscle Satellite Cells. *Curr. Genomics* **20**, 24–37 (2019).
10. Dohmen, R. G. J. *et al.* Muscle-derived fibro-adipogenic progenitor cells for production of cultured bovine adipose tissue. *Npj Sci. Food* **6**, 6 (2022).
11. Reiss, J., Robertson, S. & Suzuki, M. Cell Sources for Cultivated Meat: Applications and Considerations throughout the Production Workflow. *Int. J. Mol. Sci.* **22**, 7513 (2021).
12. Giordani, L. *et al.* High-Dimensional Single-Cell Cartography Reveals Novel Skeletal Muscle-Resident Cell Populations. *Mol. Cell* **74**, 609-621.e6 (2019).
13. De Micheli, A. J., Spector, J. A., Elemento, O. & Cosgrove, B. D. A reference single-cell transcriptomic atlas of human skeletal muscle tissue reveals bifurcated muscle stem cell populations. *Skelet. Muscle* **10**, 19 (2020).
14. De Micheli, A. J. *et al.* Single-Cell Analysis of the Muscle Stem Cell Hierarchy Identifies Heterotypic Communication Signals Involved in Skeletal Muscle Regeneration. *Cell Rep.* **30**, 3583-3595.e5 (2020).
15. Rubenstein, A. B. *et al.* Single-cell transcriptional profiles in human skeletal muscle. *Sci. Rep.* **10**, 229 (2020).

431 16. Williams, K., Yokomori, K. & Mortazavi, A. Heterogeneous Skeletal Muscle Cell and
432 Nucleus Populations Identified by Single-Cell and Single-Nucleus Resolution Transcriptome
433 Assays. *Front. Genet.* **13**, (2022).
434 17. Cornelison, D. D. W. Context Matters: In Vivo and In Vitro Influences on Muscle Satellite
435 Cell Activity. *J. Cell. Biochem.* **105**, 663–669 (2008).
436 18. Khodabukus, A., Prabhu, N., Wang, J. & Bursac, N. In Vitro Tissue-Engineered Skeletal
437 Muscle Models for Studying Muscle Physiology and Disease. *Adv. Healthc. Mater.* **7**,
438 e1701498 (2018).
439 19. Cao, J. *et al.* A human cell atlas of fetal gene expression. *Science* **370**, eaba7721
440 (2020).
441 20. Joe, A. W. B. *et al.* Muscle injury activates resident fibro/adipogenic progenitors that
442 facilitate myogenesis. *Nat. Cell Biol.* **12**, 153–163 (2010).
443 21. Proietti, D. *et al.* Activation of skeletal muscle–resident glial cells upon nerve injury. *JCI*
444 *Insight* **6**, e143469.
445 22. Ding, S. *et al.* Maintaining bovine satellite cells stemness through p38 pathway. *Sci.*
446 *Rep.* **8**, 10808 (2018).
447 23. Sherwood, R. I. *et al.* Isolation of Adult Mouse Myogenic Progenitors: Functional
448 Heterogeneity of Cells within and Engrafting Skeletal Muscle. *Cell* **119**, 543–554 (2004).
449 24. Ben-Arye, T. *et al.* Textured soy protein scaffolds enable the generation of three-
450 dimensional bovine skeletal muscle tissue for cell-based meat. *Nat. Food* **1**, 210–220 (2020).
451 25. Wang, X. & Zhou, L. The Many Roles of Macrophages in Skeletal Muscle Injury and
452 Repair. *Front. Cell Dev. Biol.* **10**, (2022).
453 26. Cantini, M. *et al.* Macrophages Regulate Proliferation and Differentiation of Satellite
454 Cells. *Biochem. Biophys. Res. Commun.* **202**, 1688–1696 (1994).
455 27. Rosenblatt, J. D., Lunt, A. I., Parry, D. J. & Partridge, T. A. Culturing satellite cells from
456 living single muscle fiber explants. *In Vitro Cell. Dev. Biol. Anim.* **31**, 773–779 (1995).
457 28. Barczyk, M., Carracedo, S. & Gullberg, D. Integrins. *Cell Tissue Res.* **339**, 269 (2009).
458 29. Gal-Levi, R., Leshem, Y., Aoki, S., Nakamura, T. & Halevy, O. Hepatocyte growth factor
459 plays a dual role in regulating skeletal muscle satellite cell proliferation and differentiation.
460 *Biochim. Biophys. Acta* **1402**, 39–51 (1998).
461 30. González, M. N. *et al.* HGF potentiates extracellular matrix-driven migration of human
462 myoblasts: involvement of matrix metalloproteinases and MAPK/ERK pathway. *Skelet.*
463 *Muscle* **7**, 20 (2017).
464 31. Hubalek, S., Post, M. J. & Moutsatsou, P. Towards resource-efficient and cost-efficient

465 cultured meat. *Curr. Opin. Food Sci.* **47**, 100885 (2022).
466 32. Bellani, C. F. *et al.* Scale-Up Technologies for the Manufacture of Adherent Cells. *Front.*
467 *Nutr.* **7**, (2020).
468 33. Machado, L. *et al.* Tissue damage induces a conserved stress response that initiates
469 quiescent muscle stem cell activation. *Cell Stem Cell* **28**, 1125-1135.e7 (2021).
470 34. Zammit, P. S. *et al.* Muscle satellite cells adopt divergent fates: a mechanism for self-
471 renewal? *J. Cell Biol.* **166**, 347–357 (2004).
472 35. Dell'Orso, S. *et al.* Single cell analysis of adult mouse skeletal muscle stem cells in
473 homeostatic and regenerative conditions. *Dev. Camb. Engl.* **146**, dev174177 (2019).
474 36. Zeng, W. *et al.* Single-nucleus RNA-seq of differentiating human myoblasts reveals the
475 extent of fate heterogeneity. *Nucleic Acids Res.* **44**, e158 (2016).
476 37. Trapnell, C. *et al.* The dynamics and regulators of cell fate decisions are revealed by
477 pseudotemporal ordering of single cells. *Nat. Biotechnol.* **32**, 381–386 (2014).
478 38. Sousa-Victor, P. *et al.* Geriatric muscle stem cells switch reversible quiescence into
479 senescence. *Nature* **506**, 316–321 (2014).
480 39. Carlson, M. E. *et al.* Molecular aging and rejuvenation of human muscle stem cells.
481 *EMBO Mol. Med.* **1**, 381–391 (2009).
482 40. Fiore, D. *et al.* Pharmacological blockage of fibro/adipogenic progenitor expansion and
483 suppression of regenerative fibrogenesis is associated with impaired skeletal muscle
484 regeneration. *Stem Cell Res.* **17**, 161–169 (2016).
485 41. Uezumi, A. *et al.* Fibrosis and adipogenesis originate from a common mesenchymal
486 progenitor in skeletal muscle. *J. Cell Sci.* **124**, 3654–3664 (2011).
487 42. Kolkmann, A., Essen, A., Post, M. & Moutsatsou, P. Development of a Chemically
488 Defined Medium for in vitro Expansion of Primary Bovine Satellite Cells. *Front. Bioeng.*
489 *Biotechnol.* **10**, (2022).
490 43. Kang, H. M. *et al.* Multiplexed droplet single-cell RNA-sequencing using natural genetic
491 variation. *Nat. Biotechnol.* **36**, 89–94 (2018).
492 44. Hafemeister, C. & Satija, R. Normalization and variance stabilization of single-cell RNA-
493 seq data using regularized negative binomial regression. *Genome Biol.* **20**, 296 (2019).
494 45. Hao, Y. *et al.* Integrated analysis of multimodal single-cell data. *Cell* **184**, 3573-3587.e29
495 (2021).
496 46. McInnes, L., Healy, J. & Melville, J. UMAP: Uniform Manifold Approximation and
497 Projection for Dimension Reduction. Preprint at https://doi.org/10.48550/arXiv.1802.03426
498 (2020).

499 47. Stuart, T. *et al.* Comprehensive Integration of Single-Cell Data. *Cell* **177**, 1888-1902.e21
500 (2019).
501 48. Thul, P. J. *et al.* A subcellular map of the human proteome. *Science* **356**, eaal3321
502 (2017).
503 49. Gene Ontology Consortium. The Gene Ontology resource: enriching a GOld mine.
504 *Nucleic Acids Res.* **49**, D325–D334 (2021).
505 50. La Manno, G. *et al.* RNA velocity of single cells. *Nature* **560**, 494–498 (2018).
506 51. Bergen, V., Lange, M., Peidli, S., Wolf, F. A. & Theis, F. J. Generalizing RNA velocity to
507 transient cell states through dynamical modeling. *Nat. Biotechnol.* **38**, 1408–1414 (2020).

Acknowledgements

We would like to thank Latifa Karim, Wouter Coppieters, Alice Mayer and Manon Deckers (GIGA institute, ULiège) for support in the acquisition and analysis of scRNA-seq data, Benjamin Bouchet for advice on immunofluorescent stainings, Christoph Börlin for help with RNA velocity analysis and Dhruv Raina for critical feedback on the manuscript.

Author contributions

TM, RGJD, LS, LM, RH and MG performed experiments and analysis. MJP and JEF supervised the study. TM and JEF wrote the manuscript with input from all authors.

Competing interests

TM, RGJD, LS, LM, RH, MG and JEF are employees of Mosa Meat B.V. MJP is co-founder and stakeholder of Mosa Meat B.V. Study was funded by Mosa Meat B.V. Mosa Meat B.V. has patents on serum-free proliferation medium (PCT/P125933PC00) and the use of cell-type selective media for cultured/cultivated meat production (N2032514, pending). All authors declare no other competing interests.

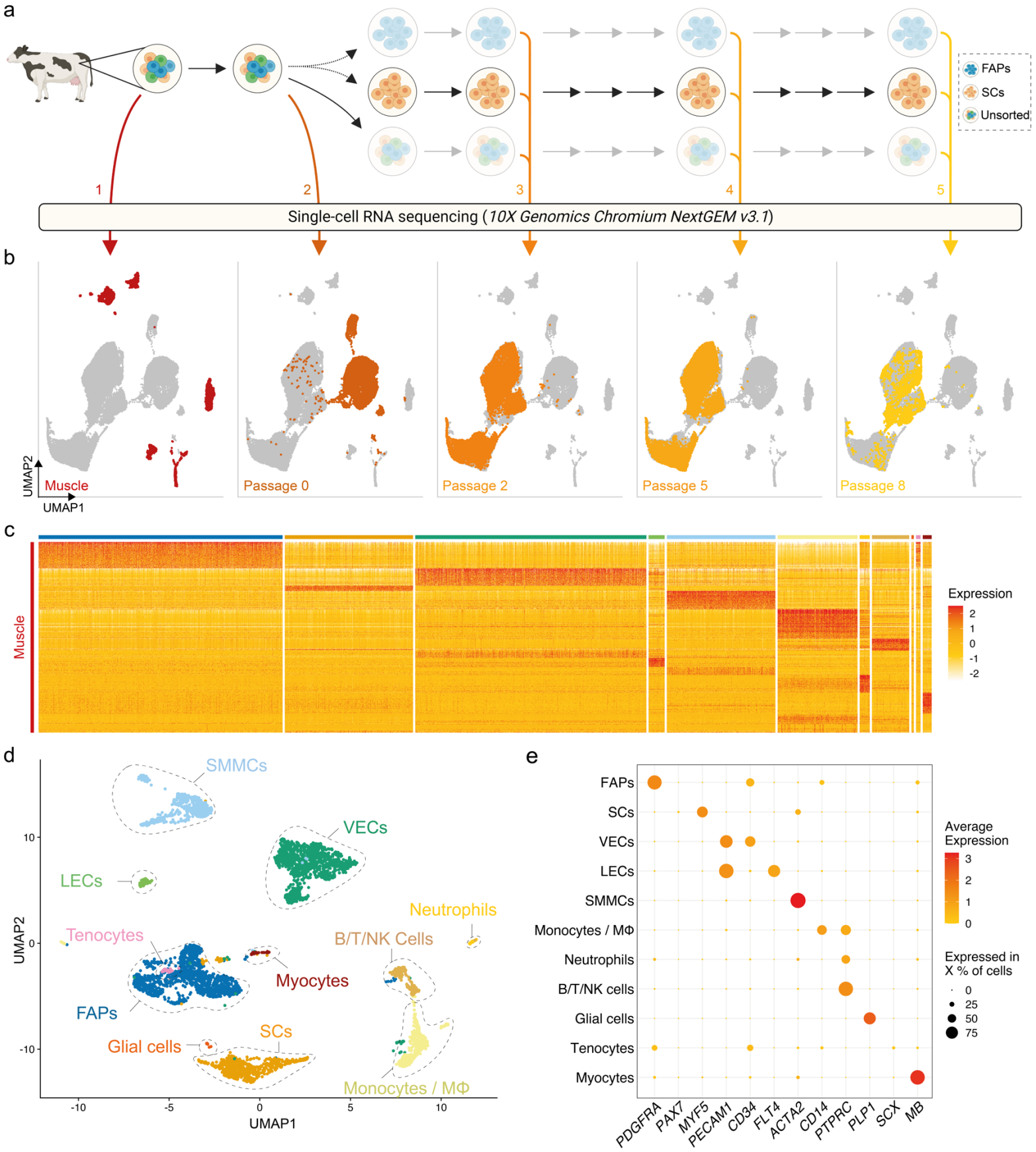
a
FAPs
SCs
Unsorted
1
2
3
4
5
Single-cell RNA sequencing (10X Genomics Chromium NextGEM v3.1)
b
UMAP2
UMAP1
Muscle
Passage 0
Passage 2
Passage 5
Passage 8
c
Muscle
Expression
2
1
0
-1
-2
d
SMMCs
VECs
LECs
Neutrophils
Tenocytes
B/T/NK Cells
Myocytes
FAPs
SCs
Glial cells
Monocytes / MΦ
UMAP2
UMAP1
10
0
-10
-10
-5
0
5
10
e
FAPs
SCs
VECs
LECs
SMMCs
Monocytes / MΦ
Neutrophils
B/T/NK cells
Glial cells
Tenocytes
Myocytes
PDGFRA
PAX7
MYF5
PECAM1
CD34
FLT4
ACTA2
CD14
PTPRC
PLP1
SCX
MB
Average Expression
3
2
1
0
Expressed in X % of cells
0
25
50
75

525 **Figure 1: Single-cell RNA sequencing of bovine muscle and muscle-derived cell**
526 **cultures.**

527 a) Overview of experimental design; coloured arrows and numerals indicate timepoints of
528 RNA sequencing of single cells isolated from bovine muscle (Timepoint 1), at passage 0
529 after 72 h in serum-free growth medium (2) and at passages 2, 5 and 8 (3, 4 and 5
530 respectively); solid arrows indicate passaging, dotted arrows indicate FACS sorting;
531 b) Combined UMAP plots showing single cells (individual points) from all five experimental
532 timepoints; clustering is based on first 30 principal components, cells from each
533 timepoint are coloured in each respective plot;
534 c) Heatmap displaying normalised expression of significantly upregulated genes in each
535 cluster identified in Timepoint 1.
536 d) UMAP of Timepoint 1; cells are coloured and clusters labelled for their assigned cell
537 types;
538 e) Dotplot showing normalised expression of cell-type specific genes, averaged within each
539 population; dot size indicates percentage of cells expressing the respective gene with at
540 least 1 count.

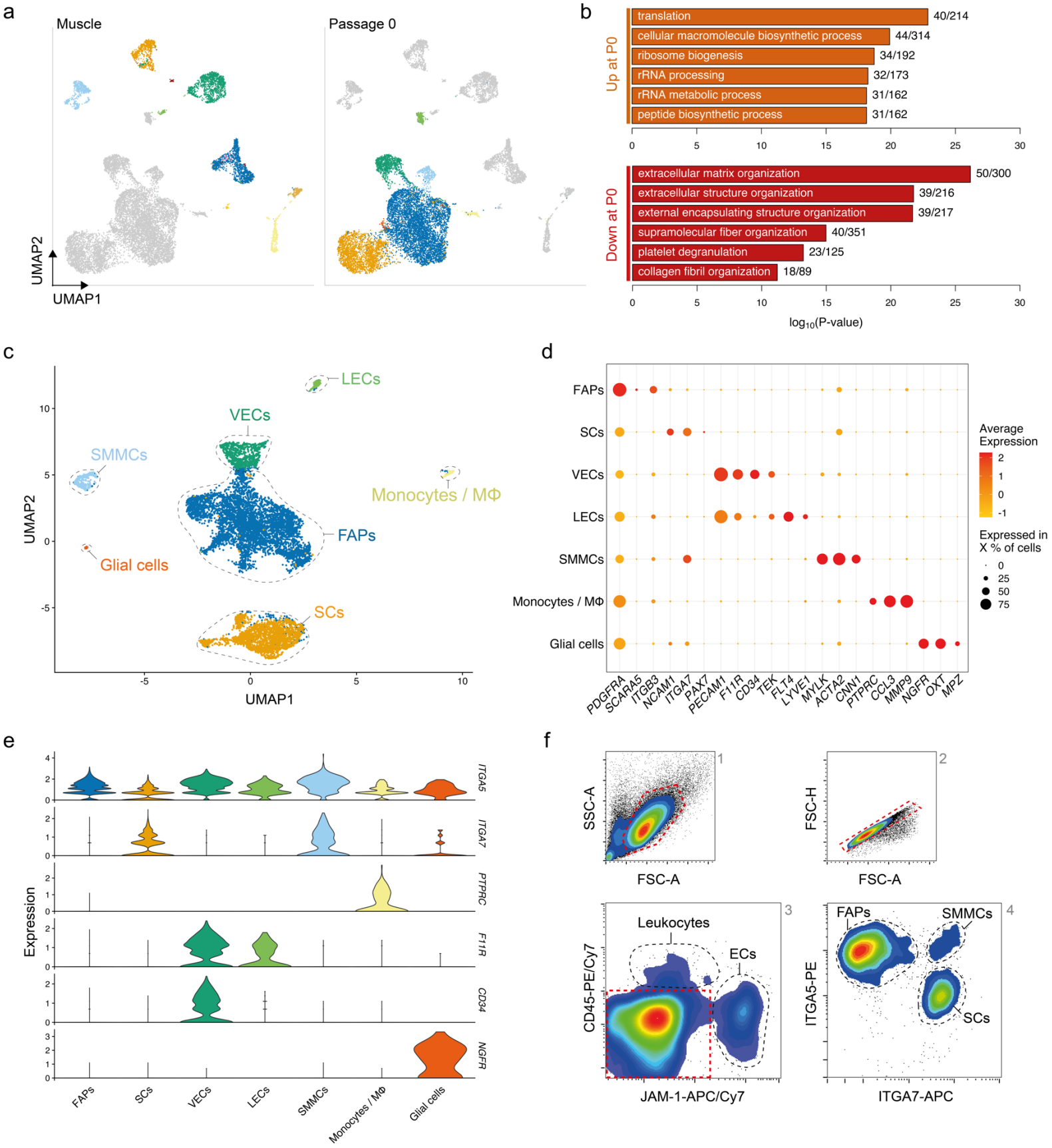
a
Muscle
Passage 0
UMAP2
UMAP1
b
Up at P0
translation 40/214
cellular macromolecule biosynthetic process 44/314
ribosome biogenesis 34/192
rRNA processing 32/173
rRNA metabolic process 31/162
peptide biosynthetic process 31/162
Down at P0
extracellular matrix organization 50/300
extracellular structure organization 39/216
external encapsulating structure organization 39/217
supramolecular fiber organization 40/351
platelet degranulation 23/125
collagen fibril organization 18/89
log10(P-value)
c
LECs
VECs
SMMCs
Monocytes / MΦ
FAPs
Glial cells
SCs
UMAP2
UMAP1
d
FAPs
SCs
VECs
LECs
SMMCs
Monocytes / MΦ
Glial cells
PDGFRA SCARA5 ITGB3 NCAM1 ITGA7 PAX7 PECAM1 F11R CD34 TEK FLT4 LYVE1 MYLK ACTA2 CNN1 PTPRC CCL3 MMP9 NGFR OXT MPZ
Average Expression
Expressed in X % of cells
e
ITGA5
ITGA7
PTPRC
F11R
CD34
NGFR
Expression
FAPs SCs VECs LECs SMMCs Monocytes / MΦ Glial cells
f
SSC-A
FSC-A
FSC-H
CD45-PE/Cy7
JAM-1-APC/Cy7
Leukocytes
ECs
ITGA5-PE
ITGA7-APC
FAPs
SMMCs
SCs

542 **Figure 2: Transcriptomic analysis defines adherent cell types with distinct**
543 **immunosurface phenotypes.**

544 a) Combined UMAP of Timepoints 1 and 2, coloured for populations in Timepoint 1 (left) or
545 2 (right), respectively;
546 b) Top five most significantly enriched GO terms corresponding to differentially expressed
547 genes up- (top) or downregulated (bottom) between Timepoints 1 and 2, after regressing
548 out the effect of cell type;
549 c) UMAP of Timepoint 2; cells are coloured and clusters labelled for their assigned cell
550 types;
551 d) Normalised gene expression of canonical markers in each population at Timepoint 2;
552 e) Violin plots showing expression of surface markers in different cell types at Timepoint 2;
553 f) Representative flow cytometry contour plots showing gating strategy for purification of
554 cell types; red dashed lines indicate gates for the subsequent plot (from 1 to 4); black
555 dashed lines indicate sorting gates for the labelled populations.

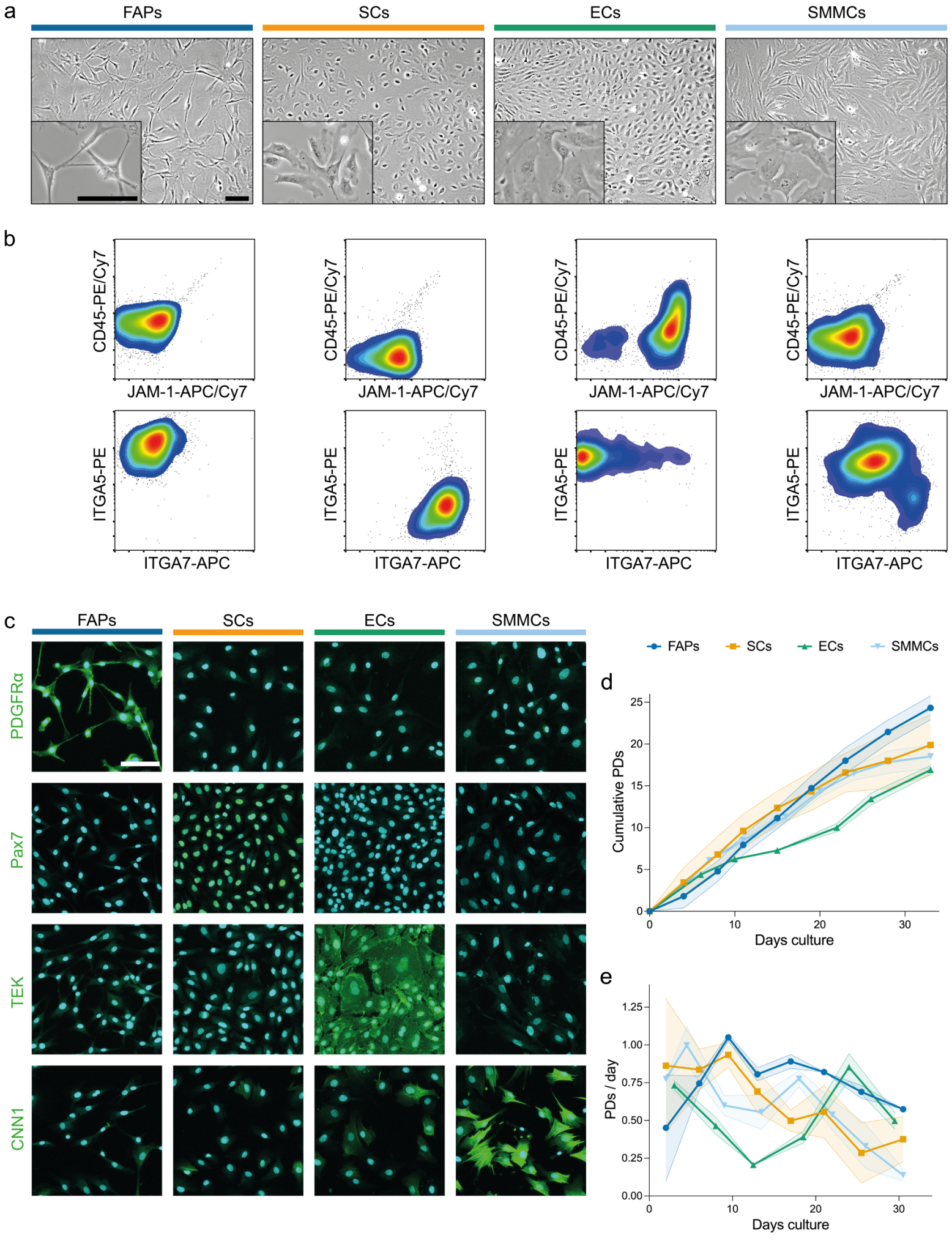
a
FAPs
SCs
ECs
SMMCs
b
CD45-PE/Cy7
JAM-1-APC/Cy7
ITGA5-PE
ITGA7-APC
c
PDGFRα
Pax7
TEK
CNN1
d
Cumulative PDs
Days culture
e
PDs / day
Days culture

557 **Figure 3: Four muscle-derived cell types can be purified and expanded in long-term**
558 **culture.**

559 a) Brightfield microscopy images of purified FAPs (blue), SCs (orange), ECs (green) and
560 SMMCs (light blue) in vitro; scale bars = 100 µm;
561 b) Flow cytometry plots of purified cell types stained for CD45/JAM-1 (top) and
562 ITGA5/ITGA7 (bottom);
563 c) Immunofluorescent staining for PDGFRα, Pax7, TEK and CNN1 (green) in purified cell
564 types; nuclei stained with Hoechst (cyan); scale bar = 100 µm;
565 d) Long-term growth curves of purified cell types in vitro, shown as cumulative population
566 doublings (PDs); shaded areas indicate standard deviation (*SD*), n = 3;
567 e) Growth rates for long-term growth experiments shown in d), shown as PDs per day, n =
568 3.

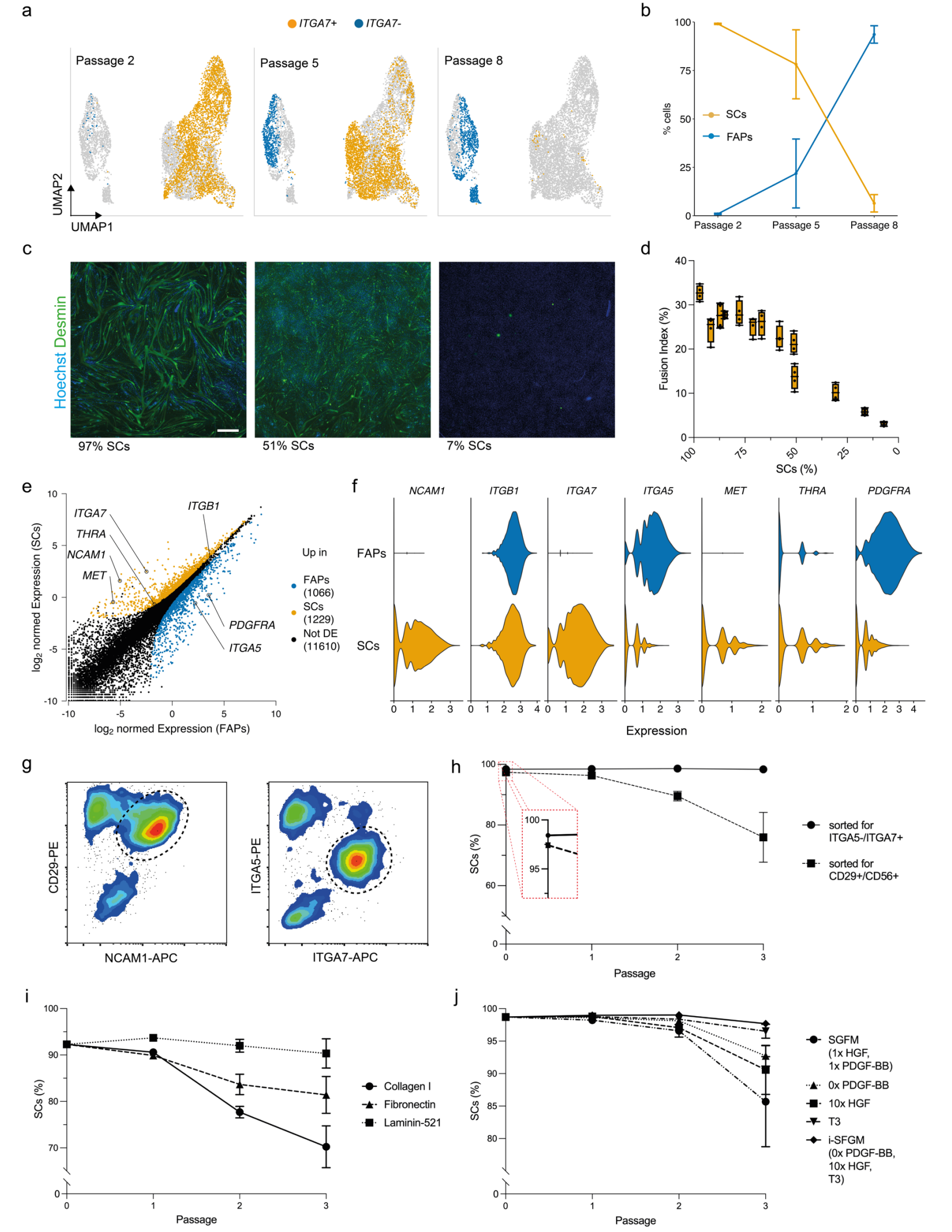
a
ITGA7+
ITGA7-
Passage 2
Passage 5
Passage 8
UMAP2
UMAP1
b
% cells
SCs
FAPs
Passage 2
Passage 5
Passage 8
c
Hoechst Desmin
97% SCs
51% SCs
7% SCs
d
Fusion Index (%)
SCs (%)
e
ITGA7
THRA
NCAM1
MET
ITGB1
PDGFRA
ITGA5
log2 normed Expression (SCs)
log2 normed Expression (FAPs)
Up in
FAPs (1066)
SCs (1229)
Not DE (11610)
f
NCAM1
ITGB1
ITGA7
ITGA5
MET
THRA
PDGFRA
FAPs
SCs
Expression
g
CD29-PE
NCAM1-APC
ITGA5-PE
ITGA7-APC
h
SCs (%)
Passage
sorted for ITGA5-/ITGA7+
sorted for CD29+/CD56+
i
SCs (%)
Passage
Collagen I
Fibronectin
Laminin-521
j
SCs (%)
Passage
SGFM (1x HGF, 1x PDGF-BB)
0x PDGF-BB
10x HGF
T3
i-SFGM (0x PDGF-BB, 10x HGF, T3)

570 **Figure 4: Optimised culture conditions prevent overgrowth of SCs.**

571 a) Combined UMAPs of sorted SCs at passages 2 (Timepoint 3, left), 5 (Timepoint 4,
572 centre) and 8 (Timepoint 5, right); clusters in respective passages are coloured for
573 *ITGA7* expression;
574 b) Proportion of SCs (*ITGA7*+) during long-term culture; error bars indicate *SD*, n = 3;
575 c) Immunofluorescent staining of cultures with varying proportions of SCs for desmin
576 (green) and Hoechst (blue) after 72 h in serum-free myogenic differentiation media;
577 scale bar = 100 µm;
578 d) Fusion indices (nuclei within desmin-stained areas as a proportion of total nuclei)
579 corresponding to c), shown as box plots, n = 4;
580 e) Normalised gene expression in SCs and FAPs at passage 2 (Timepoint 3). Points
581 represent genes, which are coloured if significantly (FDR < 0.05, log-FC > 1)
582 upregulated in FAPs (blue) or SCs (orange). Selected genes are annotated.
583 f) Violin plots showing expression of differentially expressed receptors in SCs and FAPs at
584 passage 2;
585 g) Flow cytometry plots of muscle-derived cells after 72 h in SFGM stained for
586 ITGA5/ITGA7 (left) or CD29/NCAM1 (right) prior to FACS; cells are shown after removal
587 of doublets, CD45+ and JAM-1+ cells; dashed lines indicated gating strategy for sorting;
588 h) Proportion of SCs purified with FACS protocols shown in g) during long-term culture, as
589 measured by flow cytometry; error bars indicate *SD*, n = 3;
590 i) Proportion of SCs during long-term culture on different coatings as indicated, n = 3;
591 j) As i), but for different media formulations as indicated, n = 3.

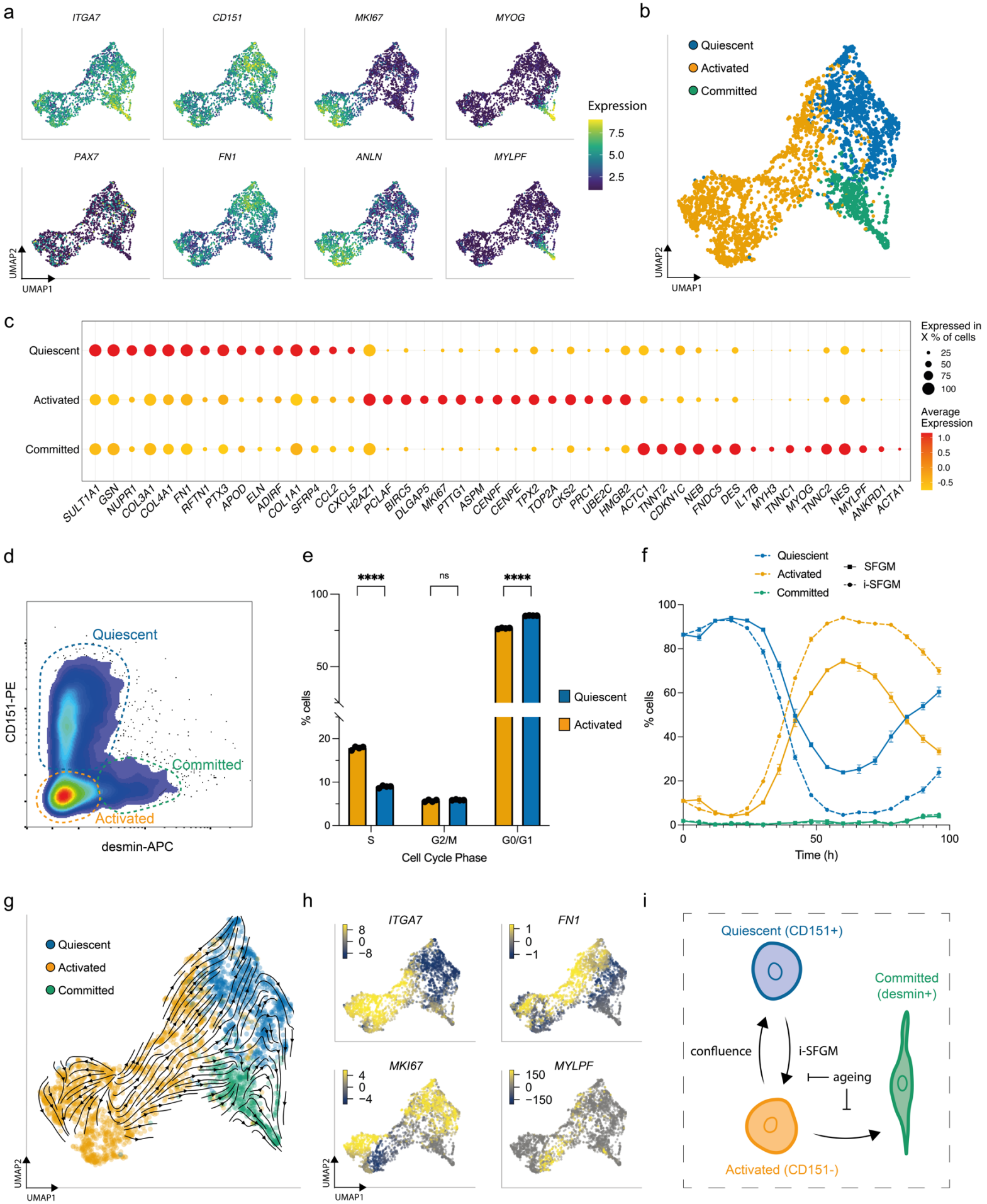
a
ITGA7
CD151
MKI67
MYOG
PAX7
FN1
ANLN
MYLPF
Expression
7.5
5.0
2.5
UMAP2
UMAP1
b
Quiescent
Activated
Committed
UMAP2
UMAP1
c
Quiescent
Activated
Committed
SULT1A1 GSN NUPR1 COL3A1 COL4A1 FN1 RFTN1 PTX3 APOD ELN ADIRF COL1A1 SFRP4 CCL2 CXCL5 H2AZ1 PCLAF BIRC5 DLGAP5 MKI67 PTTG1 ASPM CENPF CENPE TPX2 TOP2A CKS2 PRC1 UBE2C HMGB2 ACTC1 TNNT2 CDKN1C NEB FNDC5 DES IL17B MYH3 TNNC1 MYOG TNNC2 NES MYLPF ANKRD1 ACTA1
Expressed in X % of cells
25
50
75
100
Average Expression
1.0
0.5
0.0
-0.5
d
Quiescent
Committed
Activated
CD151-PE
desmin-APC
e
****
ns
****
% cells
Quiescent
Activated
S
G2/M
G0/G1
Cell Cycle Phase
f
Quiescient
Activated
Committed
SFGM
i-SFGM
% cells
Time (h)
g
Quiescent
Activated
Committed
UMAP2
UMAP1
h
ITGA7
FN1
MKI67
MYLPF
UMAP2
UMAP1
i
Quiescent (CD151+)
Committed (desmin+)
confluence
i-SFGM
ageing
Activated (CD151-)

593 **Figure 5: SCs switch dynamically between three cellular states in vitro.**

594 a) UMAPs of SCs at passage 2 (Timepoint 3), coloured by expression of indicated genes;
595 b) UMAP as a), but labelled according to SC state;
596 c) Normalised expression of the 15 most upregulated genes, averaged within SCs in each
597 state;
598 d) Flow cytometry plot of purified SCs stained for CD151 and desmin; dashed gates
599 indicate the respective cell states;
600 e) Cell cycle analysis of CD151+ (blue) and CD151- cells (orange) determined via flow
601 cytometry using the gating strategy in Supplementary Fig. 5e;
602 f) Proportion of activated, quiescent and committed SCs over one passage in SFGM or i-
603 SFGM media, as determined via flow cytometry;
604 g) UMAP as b), with averaged RNA velocity vectors embedded;
605 h) UMAPs as a), coloured by RNA velocities of denoted genes;
606 i) Dynamic model of SC states in vitro; arrows indicate direction(s) of proposed transitions
607 between states.